Simulation of the Burgers equation by NMR quantum-information processing

Zhiying Chen,[1] Jeffrey Yepez,[2] and David G. Cory[1,*]
[1]*Department of Nuclear Engineering, Massachusetts Institute of Technology, Cambridge, Massachusetts 02139, USA*
[2]*Air Force Research Laboratory, Hanscom Field, Massachusetts 01731, USA*
(Received 26 May 2005; published 23 October 2006)

We report on the implementation of Burgers equation as a type-II quantum computation on a NMR quantum-information processor. Since the flow field evolving under the Burgers equation develops sharp features over time, this is a better test of liquid-state NMR implementations of type-II quantum computers than the previous examples using the diffusion equation. In particular, we show that Fourier approximations used in the encoding step are not the dominant error. Small systematic errors in the collision operator accumulate and swamp all other errors. We propose, and demonstrate, that the accumulation of this error can be avoided to a large extent by replacing the single collision operator with a set of operators with random errors and similar fidelities. Experiments have been implemented on 16 two-qubit sites for eight successive time steps for the Burgers equation.

DOI: 10.1103/PhysRevA.74.042321 PACS number(s): 03.67.Lx, 47.11.−j, 05.60.−k

I. INTRODUCTION

Difficult nonlinear classical computational problems can be solved by using a hybrid classical-quantum device, a type-II quantum computer [1,2]. Such a device is essentially an array of small quantum-information processors (QIPs) sharing information through classical channels. Nuclear magnetic resonance (NMR) spectroscopy has proven to be a useful test bed for QIP, and in particular we have shown that a lattice of parallel QIPs can be mapped onto a spin system by creating a correspondence between the lattice sites and spatially distinct spin ensembles. A first proof of concept for numerically predicting the time-dependent solution of the classical partial differential equation with dissipative terms using our NMR technique was demonstrated for the diffusion equation [3,4].

One of the most important challenges in implementing a useful type-II quantum architecture is to avoid the accumulation of systematic errors. In the NMR implementations to date there are two important sources of systematic errors: (1) a linear approximation relating the excited magnetization to the Fourier components of the shaped rf pulse; and (2) errors from the repeated collision operators. Here we explore the impact of these errors on a simple computation and illustrate a simple way of reducing the accumulated error.

The ensemble nature of the spin system allows us to split the sample into a spatial array of lattice sites. Well-developed methods from magnetic resonance imaging allow us to selectively address the spins in each of these sites. Typically this addressing procedure is carried out in a space reciprocal to the spatial mapping, called k space, where k is the wave number of the corresponding Fourier components. The k-space formalism [5] provides a recipe for writing a spatially varying spin rotation across an ensemble of spins that have been distinguished from each other by a magnetic field gradient. The k-space formalism is essentially the application of shaped radio frequency (rf) pulses in the presence of a linear magnetic gradient field as a means of exciting selective frequencies. For most studies, the full k-space formalism is not employed and a linear approximation is invoked. If the rotation angle of the shaped pulse is small, then the excited magnetization may be accurately calculated only to first order in that angle, and the excited magnetization is related to the rf wave form simply by a Fourier transform. As a result, the required rf wave form can also be determined by taking the inverse Fourier transform of the desired initial magnetization. This technique allows us to encode arbitrary magnetization profiles spanning the various spatial locations in our experiment and thereby approximate any desired initial condition. In the previously implemented type-II quantum algorithm for the diffusion equation, higher-order Fourier components of the number density are attenuated by the dynamics and the solution is stable even in the presence of substantial accumulated errors.

To push the development of type-II implementations, we have chosen to explore the nonlinear Burgers equation to test the breakdown of the Fourier approximation. Over time, a shock front forms and high spatial frequencies in the magnetization profile become important and it is these high spatial frequencies that we expect are most sensitive to errors. The numerical treatment of the quantum lattice gas (QLG) algorithm for the Burgers equation [6] therefore offers a stronger proof of our NMR quantum-computing approach since the effect of the nonlinear convective term in the equation generates a sharp edge as a shock develops in time that is not mimicked by spin relaxation, random self-diffusion, or rf inhomogeneities. In addition, we demonstrate shock formation driven by a tunable viscosity parameter to show that the width of the shock front is not determined by implementation imperfections.

The first-order accurate Fourier approximation was expected to be the dominant error source in the NMR implementation. However, NMR simulations with controlled errors shows that the systematic error induced by the experimental implementation of the unitary collision operator associated with the QLG algorithm is the major challenge. Replacing the single collision operator with a set of

*Electronic address: jeffrey.yepez@hanscom.af.mil; URL: http://qubit.plh.af.mil

operators to randomize errors allows us to improve the robustness of the implementation.

II. TYPE-II QUANTUM ALGORITHM

A quantum lattice gas is a system of quantum particles moving and colliding on a discrete space-time lattice. This quantum particle system is isomorphic to a lattice-based qubit system with local qubit-qubit interactions and local transfer of qubit states between neighboring spatial nodes. The mapping is as follows: the probability of a particle residing at a particular lattice node is equated to the moduli squared of the probability amplitude of a qubit at a unique location being in its excited quantum state. That is, each spatial location that a particle may occupy is mapped onto a qubit associated with a unique location.

The dynamics of the evolution in the QLG algorithm is described at three scales: the microscopic, mesoscopic, and macroscopic scales. At the microscopic scale, the local microscopic quantum state of the qubits at time t located within the quantum node at position z is denoted by $|\psi(z,t)\rangle$. The local microscopic quantum-mechanical evolution equation can be written as follows:

$$|\psi(z,t+\Delta t)\rangle = \hat{\mathcal{S}}\hat{\mathcal{G}}\hat{\mathcal{C}}|\psi(z,t)\rangle, \tag{1}$$

where $\hat{\mathcal{S}}$ is the streaming operator (orthogonal transformation), $\hat{\mathcal{G}}$ is a projection operator representing the measurement process (nonunitary transformation), and $\hat{\mathcal{C}}$ is the collision operator (unitary transformation). Equation (1) reduces to linear Schrödinger evolution when the operator $\hat{\mathcal{G}}$ is the identity operator. Each particle moves along the lattice and, in a one-dimensional chain of qubits, only left-moving and right-moving qubits are needed to encode this particle motion. The stream operator $\hat{\mathcal{S}}$ models this particle motion by transferring qubit states between neighboring quantum nodes in the $(1+1)$-dimensional construction. A simplified qubit-qubit interaction, represented by the unitary operator $\hat{\mathcal{C}}$, allows a particle to change its direction of motion (via a *collision* with another particle) or keep moving at constant speed in its original direction of motion.

One can describe the dynamical behavior of this many-body system of particles at the mesosopic scale by determining their occupation probabilities on the lattice points. The mesoscopic dynamical behavior of the system is modeled by a finite-difference form of the quantum Boltzmann equation:

$$\left(\partial_t \pm \frac{\Delta z}{\Delta t}\partial_z + \frac{1}{2}\frac{\Delta z^2}{\Delta t}\partial_{zz}\right) f_{\pm}(z,t) = \pm \frac{1}{\Delta t}\Omega(f_+,f_-), \tag{2}$$

where the collision function is

$$\Omega(f_+,f_-) = \sin^2\theta(f_- - f_+) + \sin 2\theta \cos(\zeta - \xi) \times \sqrt{f_+(1-f_+)f_-(1-f_-)}, \tag{3}$$

and where the angles θ, ζ, and ξ parametrize the SU(2) unitary quantum-mechanical interaction between states $|01\rangle$ and $|10\rangle$ in the zero-quantum subspace [6–8]. Because the projection operator $\hat{\mathcal{G}}$ demolishes the local quantum state, previously entangled by $\hat{\mathcal{C}}$, the stream operator $\hat{\mathcal{S}}$ can be implemented at the mesoscopic scale by directly transferring occupation probabilities, in place of quantum-mechanically transferring qubit states. That is, the stream operator can be accomplished at either the meso- or microscopic scale; yet in our NMR implementation of the type-II quantum algorithm, it is practical to represent the streaming operation directly at the mesoscopic scale, in fact by implementing this operation on a host classical computer.

Finally, to bridge to the macroscopic scale, the occupation probabilities of the particles residing at each lattice site are summed together to determine the number density (number of particles per unit nodal volume):

$$\rho(z,t) = f_+(z,t) + f_-(z,t), \tag{4}$$

and the flow speed in the Burgers equation (6) is

$$u(z,t) = c[\rho(z,t) - 1], \tag{5}$$

where the unit speed in the QLG model is $c \equiv \frac{\Delta z}{\Delta t}$. These macroscopic field quantities ρ and u, defined over the lattice nodes, become continuous fields as the lattice resolution approaches infinity ($\Delta t \to 0$ and $\Delta x \to 0$), which is called the *continuum limit*. Through a Chapman-Enskog perturbation expansion applied in the continuum limit, from the quantum Boltzmann equation emerges the Burgers equation, an effective field theory that is parabolic in time and space and nonlinear in $u(z,t)$ [7]:

$$\partial_t u(z,t) + u\partial_z u(z,t) = \nu\partial_{zz} u(z,t), \tag{6}$$

where ν is the diffusive transport coefficient for the shear viscosity. A detailed presentation of the analytical procedure of the Chapman-Enskog expansion is presented in the preceding paper treating, in detail, the QLG algorithm for the Burgers equation from a theoretical viewpoint [8]. The quantum Boltzmann equation (2) is derived from (1), and in turn the Burgers equation (6) is derived from (1) where the shear viscosity is found to be of the form [8]

$$\nu = \frac{1}{2}\frac{\Delta z^2}{\Delta t}\cot^2\theta. \tag{7}$$

That the transport coefficient is a function of θ is a salient feature of the type-II quantum algorithmic method. As $\theta \to \frac{\pi}{2}$, the flow dynamics modeled by the quantum system becomes inviscid at the macroscopic scale.

III. NMR EXPERIMENTAL IMPLEMENTATION

The QLG algorithm is initialized, in the NMR case, by encoding the particles' occupation probabilities as a spin-magnetization profile. To handle the one-dimensional Burgers equation, it is sufficient to use two qubits (two spin-$\frac{1}{2}$ nuclei) per lattice site, where each encodes a single real-valued occupation probability. A room-temperature solution of isotopically labeled chloroform ($^{13}CHCl_3$) was chosen for implementing the experiments, where the hydrogen and the labeled carbon nucleus served as qubits 1 and 2, respectively. The difference of the gyromagnetic ratio of the two spins

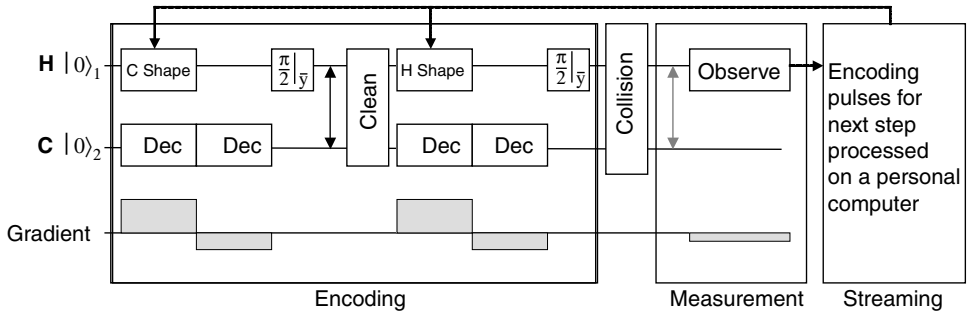

FIG. 1. QLG algorithm implemented in four steps. Three horizontal lines represent proton spin, carbon spin, and fried gradient. Both starting magnetizations are encoded in the proton channel first due to the high signal-to-noise ratio, and decoupled in the carbon channel to prevent interfering of scalar coupling. The collision operator is applied after the initialization. Measurements are also taken in two steps in the proton channel followed by data processing in a personal computer.

generates widely spaced resonant frequencies that allow us to address each spin independently.

A lattice of QIPs is related to the ensemble sample by creating a correspondence between lattice sites and spatially dependent positions in the sample. A linear magnetic field gradient is used to generate distinct spatially dependent resonant frequencies that we can distinguish and modulate by a shaped rf pulse. In this way, the magnetic field gradient allows the entire spin ensemble to be sliced into a lattice of smaller, and individually addressable, sub-ensembles.

The lattice initialization starts by transforming thermal equilibrium states into pseudopure states [9]. The equilibrium state is highly mixed and the two nuclear spins have unequal magnetizations. Thus, equalization of the magnetizations is required prior to creating the pseudopure state. The dynamical evolution is caused by a collision operator (a unitary operation), measurement (a nonunitary operation), and streaming (an orthogonal operation) according to the QLG algorithmic paradigm. The four main steps of the NMR implementation of QLG algorithm to evolve the flow field by one time step Δt are graphically depicted in Fig. 1. Beginning with the quantum state preparation and then the evolution of $f_\pm$ governed by the combined action of the collision operator, measurement, and streaming. The details of the correspondence between NMR spectroscopy, quantum computing, and the quantum Boltzmann equation pictures of the method are presented in Table I.

A. Nonunitary state preparation

Each occupation probability is mapped onto a lattice site as the expectation value of a number operator at a space-time site $n\Delta z$ at time $m\Delta t$. As a result, the initial states of the qubits are

$$|q_\pm\rangle = \sqrt{f_\pm^{\rm eq}(n\Delta z, m\Delta t)}|1_\pm\rangle_{nm} + \sqrt{1-f_\pm^{\rm eq}(n\Delta x, m\Delta t)}|0_\pm\rangle_{nm}. \tag{8}$$

The combined wave function for a lattice site is a tensor product over the qubits:

$$|\psi(n\Delta z, m\Delta t)\rangle = |q_+\rangle_{nm} \otimes |q_-\rangle_{nm} \tag{9a}$$

$$= (f_+^{\rm eq}|1_+\rangle_{nm} + \sqrt{1-f_+^{\rm eq}}|0_+\rangle_{nm}) \otimes (f_-^{\rm eq}|1_-\rangle_{nm} + \sqrt{1-f_-^{\rm eq}}|0_-\rangle_{nm}) \tag{9b}$$

$$= \sqrt{f_+^{\rm eq} f_-^{\rm eq}}|11\rangle_{nm} + \sqrt{f_+^{\rm eq}(1-f_-^{\rm eq})}|10\rangle_{nm} + \sqrt{(1-f_+^{\rm eq})f_-^{\rm eq}}|01\rangle_{nm} + \sqrt{(1-f_+^{\rm eq})(1-f_-^{\rm eq})}|00\rangle_{nm} \tag{9c}$$

$$= \begin{pmatrix} \sqrt{(1-f_+^{\rm eq})(1-f_-^{\rm eq})} \\ \sqrt{(1-f_+^{\rm eq})f_-^{\rm eq}} \\ \sqrt{f_+^{\rm eq}(1-f_-^{\rm eq})} \\ \sqrt{f_+^{\rm eq} f_-^{\rm eq}} \end{pmatrix}_{nm}. \tag{9d}$$

The initial equilibrium occupation probabilities that we use are

$$f_\pm^{\rm eq} = \frac{\rho}{2} \mp \frac{1}{2\alpha}[\sqrt{1+\alpha^2} - \sqrt{1+\alpha^2(\rho-1)^2}], \tag{10}$$

where $\alpha = \cot\theta$, for $\theta = \pi/4.882$ rad. The initial magnetization is specified by using a rf pulse shaped by the Fourier transform of the desired magnetization (transform of the initial number density profile). While applying the shaped pulse, a carbon decoupling sequence is performed to prevent the scalar coupling from interfering with the low-power shaped pulses. In addition, the $\pi/2$ pulse, which rotates the qubit state vector from the x to the z axis, is applied separately just after each initialization. This is done to keep the valuable information along the longitudinal direction where it will not be affected by the gradient and chemical shift. The encoding of initial states on both spins is accomplished in two steps: The initial carbon magnetization is recorded on the protons before being transferred to the carbons and followed by the initialization of proton magnetization. Furthermore, a short pulse sequence, called the *clean sequence*, is executed after the first SWAP gate to erase the phase distortion that may be caused by the decoupling sequence.

B. Unitary collision

During the collision step, all the nodes locally evolve according to the Schrödinger wave equation with the unitary transformation

TABLE I. Three different pictures: A single point of the system.

NMR spectroscopy	Quantum computing	Quantum Boltzmann equation
Spin-$\frac{1}{2}$ nuclei proton, carbon isotope ^{13}C	Qubit $\|q\rangle=\alpha\|0\rangle+\beta\|1\rangle$	Particle's local state $\hat{n}_\alpha$, $\hat{e}_a$
Molecule containing above nuclei, such as chloroform, alanine, dibromoproprionic acid, *trans*-crotonic acid	Microscopic quantum computer, two qubits, three qubits, four qubits, seven qubits	Site of lattice $\vec{x}$
Parcel of liquid $\sim 10^{18}$ molecules	Mesoscopic quantum computer Many quantum computers	Site of superlattice $\vec{X}$ at the mesoscopic scale
Relaxation $\varrho_{\text{thermal}}=\mathbf{1}+\varepsilon(\sigma_z^1+\sigma_z^2)$	Memory reset $\|q\rangle\rightarrow e^{-\beta E_\uparrow}\|1\rangle+e^{-\beta E_\downarrow}\|0\rangle$	State demolition
Pseudopure state $\varrho_{\text{thermal}} \xrightarrow{rf+\nabla} \mathbf{1}+\varepsilon\|\psi\rangle\langle\psi\|$	Ket $\|\psi\rangle$	Distribution function $\|\psi(\vec{x},t)\rangle\rightarrow\otimes_{a=1}^{B}\|q_a(\vec{x},t)\rangle$ $\|q_a\rangle=\sqrt{f_a}\|1\rangle+\sqrt{1-f_a}\|0\rangle$
Spin-spin interaction+rf pulse sequence $e^{-i\hat{H}_{\text{int}}\Delta t/\hbar-i\omega_x^\gamma(\Delta t)(\sigma_x^1+\sigma_x^2)\Delta t-i\omega_y^\gamma(\Delta t)(\sigma_y^1+\sigma_y^2)\Delta t}$	Logic gate $\hat{U}=e^{-i(\sigma_x\sigma_y-\sigma_y\sigma_x)\Delta t/\hbar}$	On-site collision function $\Omega_a(\vec{x},t)$
Measurement of free induction decay	Ensemble measurement $\text{Tr}[\varrho(t)\hat{n}_\alpha]$	Occupation probability $f_a(\vec{x},t)$
Gradient ∇B	Resonant frequency shift $\vec{k}\rightarrow\vec{k}+\Delta k$	Streaming $f(\vec{x})\rightarrow f(\vec{x}+\hat{e}_a)$
Magnetic resonance imaging	Array of mesoscopic quantum computers	Discrete lattice
Molecular independence	Tensor product wave function $\|\Psi\rangle=\otimes_{x=1}^{V}\|\psi(x)\rangle$	Mesoscopic ensemble of states (only local entanglement)
Homogeneously applied rf	Tensor product operator $\hat{C}=\otimes_{x=1}^{V}\hat{U}$	Parallel computation On-site collisions

$$|\psi'(n\Delta z)\rangle = e^{-i\hat{H}_{\text{NMR}}\Delta t/\hbar}|\psi(n\Delta z)\rangle. \tag{11}$$

The effective two-spin Hamiltonian (averaged dipolar interaction of the spins' magnetic moments for a freely rotating molecule) is

$$\hat{H}_{\text{NMR}} = \hbar\omega_{\text{H}}\hat{\sigma}_z^{\text{H}} + \hbar\omega_{\text{C}}\hat{\sigma}_z^{\text{C}} + J\hat{\sigma}_z^{\text{H}}\sigma_z^{\text{C}}, \tag{12}$$

where the resonant frequencies of the hydrogen and carbon-13 nuclei are $\omega_{\text{H}}=300$ MHz and $\omega_{\text{C}}=75$ MHz, respectively, and where the spin-coupling resonant frequency is much smaller, $J/\hbar=214$ Hz. The interaction part of the NMR Hamitonian, accounting for independently shaped radio frequency pulses $B_1(t)$ and $B_2(t)$ along the transverse $\hat{x}$ and $\hat{y}$ directions, has the general form

$$\begin{aligned}\hat{H}_{\text{int}}(t) = {} & \hbar\gamma_{\text{H}}B_{1x}(t)\sigma_x^{\text{H}} + \hbar\gamma_{\text{H}}B_{1y}(t)\sigma_y^{\text{H}} + \hbar\gamma_{\text{C}}B_{2x}(t)\sigma_x^{\text{C}} \\ & + \hbar\gamma_{\text{C}}B_{2y}(t)\sigma_y^{\text{C}},\end{aligned} \tag{13}$$

where the gyromagnetic ratio for the proton γ_{H} is $2.675\,222\,12\times10^8$(rad s^{-1}) T^{-1} and for the carbon-13 nucleus γ_{C} is $6.728\,286\times10^7$ (rad s^{-1}) T^{-1}.

In the double-rotating frame, only the J-coupling term in (12) remains, and the resulting collision operator that is applied to all the lattice sites independently,

$$|\psi'(n\Delta z)\rangle = \hat{\mathcal{C}}|\psi(n\Delta z)\rangle, \tag{14}$$

for all n, has the form

$$\hat{\mathcal{C}} = e^{-i\hat{H}_{\text{int}}(t)\Delta t/\hbar - i\hat{J}\hat{\sigma}_z^{\text{H}}\sigma_z^{\text{C}}T_{\text{delay}}/\hbar+\cdots}. \tag{15}$$

This is the effective unitary evolution operator that is "programmed" by decomposing it into a sequence of external rf pulses modifying the natural spin-spin scalar coupling.

According to the quantum lattice gas paradigm [8], the effective components of the unitary collision operator determines the form of the macroscopic effective field theory (a parabolic partial differential equation) and the value of its transport coefficients (particularly, the coefficient of the dissipative shear viscosity term in the case of the Burgers equation). A matrix representation of the collision operator for the Burgers equation is block diagonal:

$$\hat{\mathcal{C}} = \begin{pmatrix} 1 & 0 & 0 & 0 \\ 0 & \cos\theta & \sin\theta & 0 \\ 0 & -\sin\theta & \cos\theta & 0 \\ 0 & 0 & 0 & 1 \end{pmatrix}. \tag{16}$$

In operator form, (16) can be written as

$$\hat{\mathcal{C}} = \exp\left(-i\frac{\theta}{2}(\sigma_x^{\mathrm{H}}\sigma_y^{\mathrm{C}} - \sigma_y^{\mathrm{H}}\sigma_x^{\mathrm{C}})\right), \tag{17}$$

where the Euler angle θ is determined by the physical values of the spin-coupling energy, the delay time, and Planck's constant as follows:

$$\theta \equiv \frac{JT_{\mathrm{delay}}}{\hbar}. \tag{18}$$

The product operators in the exponent commute with each other, resulting in

$$\hat{\mathcal{C}} = \exp\left(-i\frac{\theta}{2}\sigma_x^{\mathrm{H}}\sigma_y^{\mathrm{C}}\right)\exp\left(i\frac{\theta}{2}\sigma_y^{\mathrm{H}}\sigma_x^{\mathrm{C}}\right). \tag{19}$$

Both terms can be expanded as natural scalar Hamiltonian couplings sandwiched with the appropriate single rotations, resulting in

$$\begin{aligned}\hat{\mathcal{C}} = {} & e^{-i(\pi/4)\sigma_y^{\mathrm{C}}}e^{-i(\pi/4)\sigma_x^{\mathrm{H}}}e^{-i(\theta/2)\sigma_z^{\mathrm{H}}\sigma_z^{\mathrm{C}}}e^{i(\pi/4)\sigma_x^{\mathrm{H}}}e^{i(\pi/4)\sigma_y^{\mathrm{C}}} \\ & \times e^{i(\pi/4)\sigma_x^{\mathrm{C}}}e^{-i(\pi/4)\sigma_y^{\mathrm{H}}}e^{-i(\theta/2)\sigma_z^{\mathrm{H}}\sigma_z^{\mathrm{C}}}e^{i(\pi/4)\sigma_y^{\mathrm{H}}}e^{-i(\pi/4)\sigma_x^{\mathrm{C}}},\end{aligned} \tag{20}$$

which has the form of (15). There are many ways to encode the collision operator; the pulse sequence (20) is one such example. An alternative pulse sequence with a slightly difference matrix representation from (16), but which leads to a similar quantum Boltzmann equation, is the following:

$$\begin{aligned}\hat{\mathcal{C}} = {} & e^{-i(\pi/4)(\sigma_y^{\mathrm{H}}+\sigma_y^{\mathrm{C}})}e^{-i(\pi/4)\sigma_z^{\mathrm{H}}\sigma_z^{\mathrm{C}}}e^{-i(\theta/2)(\sigma_x^{\mathrm{H}}-\sigma_x^{\mathrm{C}})} \\ & \times e^{i(\pi/4)(\sigma_y^{\mathrm{H}}+\sigma_y^{\mathrm{C}})}e^{-i(\pi/4)(\sigma_x^{\mathrm{H}}+\sigma_x^{\mathrm{C}})}e^{-i(\pi/4)\sigma_z^{\mathrm{H}}\sigma_z^{\mathrm{C}}}e^{i(\pi/4)(\sigma_x^{\mathrm{H}}+\sigma_x^{\mathrm{C}})}\end{aligned} \tag{21}$$

$$= \begin{pmatrix} 1 & 0 & 0 & 0 \\ 0 & -i\sin\theta & -i\cos\theta & 0 \\ 0 & -i\cos\theta & i\sin\theta & 0 \\ 0 & 0 & 0 & 1 \end{pmatrix}. \tag{22}$$

In (21), the value of the Euler angle θ is determined by the rf pulse shape.

In our test, we will set the shear viscosity to $\nu = 1/4$, in lattice units where $\Delta z = \Delta t = 1$. According to (7), we then choose $\theta = \pi/3.289$. Since the resonant spin-coupling angular frequency is $\omega_{\mathrm{HC}} \equiv J/\hbar = 214$ Hz for our spectrometer setup, according to (18) we use the delay time in the experiment $T_{\mathrm{delay}} = 4.46$ ms to produce the desired viscosity.

The exponential terms of single-spin rotations are implemented by $\pi/2$ and $\pi/4$ pulses. The exponents of terms with $\sigma_z^H\sigma_z^C$ represent the natural internal Hamiltonian evolutions with time period $\hbar/2J$. Here, the evolution of the internal Hamiltonian is ignored while the rf pulse is applied. This approximation leads to a systematic error that will accumulate during the course of the computation. In general, these errors are easy to avoid, but since the purpose of the investigation was to explore the sensitivity to accumulated errors we did not correct it. The collision operator follows the encoding (step 2), and it is implemented without magnetic field gradients to ensure that all of the sites in the sample undergo the same transformation.

C. Nonunitary measurement

Third, we measure the occupation probabilities. This projective nonunitary process erases all the superpositions and quantum entanglement that were created by the unitary collision operator in the second step, and ultimately gives rise to the nonlinearity in the effective macroscopic field theory, the Burgers equation with nonlinear convection [8]. In the basis of a two-qubit system, the number operators for the occupancy of qubits are defined in terms of the singleton qubit number operation $\hat{n} = \left(\begin{smallmatrix} 1 & 0 \\ 0 & 0 \end{smallmatrix}\right)$ as follows: $\hat{n}_+ = \mathbf{1} \otimes \hat{n}$ and $\hat{n}_- = \hat{n} \otimes \mathbf{1}$. Therefore, the measured occupation probability is determined as follows:

$$f_{\pm}(n\Delta z, m\Delta t) = \langle \psi(n\Delta z, m\Delta t)|\hat{n}_{\pm}|\psi(n\Delta z, m\Delta t)\rangle. \tag{23}$$

The occupation probabilities for each spin are obtained following the collision step by measuring the z magnetization according to the following equation:

$$f_{(+,-)}(n,m) = \frac{1}{2}[1 + \langle \psi(n,m)|\sigma_z^{(1,2)}|\psi(n,m)\rangle]. \tag{24}$$

Since only σ_x and σ_y are observable in our NMR spectrometer, a $\pi/2$ pulse has been used to bring the z magnetization into the transverse plane. The measurements are done in two separate experiments, where a SWAP gate is applied to bring the magnetization from the carbon to the proton channel. This SWAP operation is done because the higher signal-to-noise ratio in the proton channel allows us to improve the accuracy of our implementation. During the "readout" process (step 3), a weak magnetic field gradient is applied to distinguish different sites. The observed proton signals are digitized and Fourier transformed, allowing us to record the spatially dependent spin magnetization profile.

D. Orthogonal streaming

Fourth, and the last step of the QLG algorithm, we shift the $f_{\pm}$ obtained in the previous step to its nearest neighbor using a short MATLAB program. This step requires only classical communication between neighboring sites. The time is incremented after this step. Then, we loop back to step 1 and update the field of occupation probabilities over the lattice sites. In this way, we can continue to iterate forward in time and make a time-history record of the occupation probabilities, which in turn gives us the temporal evolution of the number density field.

IV. EXPERIMENTAL RESULTS

In our NMR quantum-information processing experiment for modeling the Burger equation, we observed deviations between the numerically predicted data points and analytically predicted solutions. These errors can be attributed to imperfections in the NMR implementation. The major error sources in the NMR implementation are known, so to explore the source and relative strength of these errors, we have

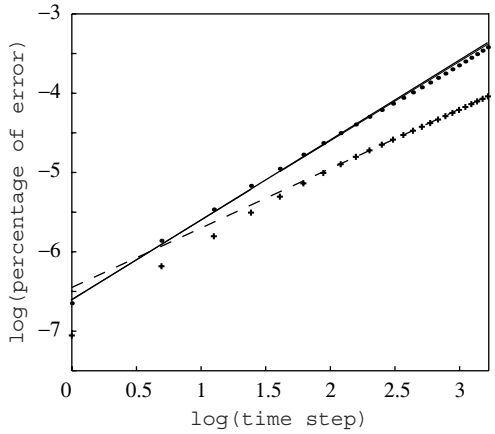

FIG. 2. The growth of the systematic errors due to the collision operator in two NMR implementation. The single-collision-operator data (dots) are fitted (solid line) with a line of slope 1, which shows linear growth of the error. The collision-operator data with modulated phases (pluses) are fitted with a line of slope 3/4 (dashed line). The buildup of the systematic errors has been slowed down by the proposed method. However, the systematic errors have not been totally converted into random errors.

simulated the NMR experiments. The major error source in this implementation is the collision operator, and it is introduced by ignoring the scalar coupling between proton and carbon during the rf pulses. When applying a rf pulse on the proton qubit, the Hamiltonian in the rotating form is $H=J\sigma_z^H\sigma_z^C+\hbar\gamma_H B_1(t)\sigma_x^H$, where B_1 is the strength of the rf pulse. With the presence of the scalar coupling, a small portion of the proton magnetization has been transferred to the carbon qubit. Therefore, the applied propagator can be recast as $U=U_{\text{desired}}U_{\text{error}}$.

The error in the collision operator is a systematic error that builds up throughout the successive time steps. Although this is not the dominant error at the beginning of the implementation, it eventually dominates the first-order error due to the Fourier approximation and becomes the dominant issue after just several time step interations. Notice that while the reduction of the initial magnetization from the Fourier transform is systematic, since the magnetization profile is changing the errors are not precisely repeated. In the collision operator, however, the errors are exactly the same from step to step. In addition we expect that the radio frequency inhomogeneity leads to strongly correlated errors in the lattice encoding. Hence, we have proposed replacing a single collision operator with a set of collision operators that have similar fidelity but randomized error terms.

Since the collision operator for the Burgers equation is a zero-order coherence term, the collision operator commutes with the rotation operator. Therefore, we apply a 90° rotation operator to the collision operator at each step to mitigate error growth. Consequently, a dramatic improvement is observed as shown in Fig. 2. On a logarithmic plot, the simulation results fitted a line with a slope of 3/4. If the error terms in the collision operators were totally randomized and hence followed a Gaussian distribution, the best-fit regression line should have had a slope of 1/2. The deviation between our simulation data and the ideal Gaussian case indicates residual systematic error in the collision operator. In a future study, we may use strongly modulated pulses to randomize the error terms.

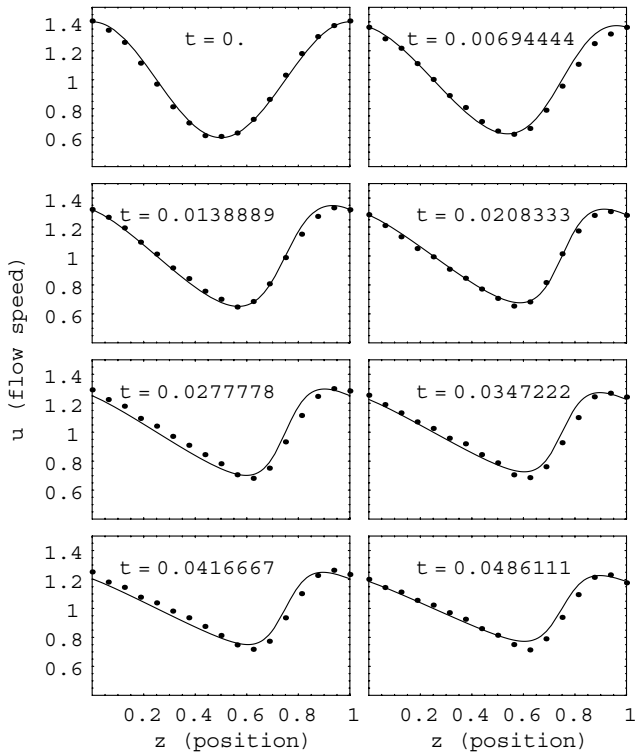

FIG. 3. The experimental data are plotted together with the analytical solutions for eight time steps on a lattice of 16 parallel two-qubit QIPs. Viscosity $\nu=\Delta z^2/4\Delta t$. Experimental NMR data (dots) versus analytical solution (curves). Randomizing the error terms in the collision operator has improved the experimental results dramatically.

The experimental number densities are overplotted in Fig. 3 with the exact analytical solutions. Eight successive time steps of the quantum algorithm were implemented on 16 two-qubit sites. An improvement of our present experimental approach using collision operators with modulated phases is observed. The agreement of the data with the analytical solutions is encouraging and suggests that totally randomizing error terms in the collision operator may offer further improvement.

V. CONCLUSION

NMR quantum simulation has provided an alternative way to study NMR spectroscopic implementations. From the simulation, we find that the major error sources are due to imperfect control of the quantum spin system and the Fourier approximation associated with setting its magnetization profile. Our proposed method for converting the systematic errors into random errors is effective. The improvement we achieve relative to the previous experiment is encouraging, and it demonstrates the possibility of using the same technique in future studies. The closeness of the numerical data

to the exact analytical results for the nonlinear Burgers equation further proves the practicality of implementing the QLG algorithm using a spatial NMR technique. In addition, although the limitation of the Fourier approximation is not dominant, the problem of precisely initializing a lattice of QIPs still remains an open issue.

ACKNOWLEDGMENTS

We thank M. A. Pravia, N. Boulant, H. Cho, Y. Liu, and P. J. Love for valuable discussion. This work was supported by the Air Force Office of Scientific Research, along with DARPA, ARDA, and ARO.

[1] J. Yepez, Int. J. Mod. Phys. C **9**, 1587 (1998); G. P. Berman, A. A. Ezhov, D. I. Kamenev, and J. Yepez, Phys. Rev. A **66**, 012310 (2002).
[2] J. Yepez, Int. J. Mod. Phys. C **12**, 1273 (2001); Comput. Phys. Commun. **146**(3), 277 (2002).
[3] M. Pravia, Z. Chen, J. Yepez, and D. G. Cory, Comput. Phys. Commun. **146**, 339 (2002).
[4] M. Pravia, Z. Chen, J. Yepez, and D. G. Cory, Quantum Inf. Process. **2**, 1 (2003).
[5] A. Sodickson and D. G. Cory, Prog. Nucl. Magn. Reson. Spectrosc. **33**, 77 (1998).
[6] J. Yepez, J. Stat. Phys. **107**, 203 (2002).
[7] J. Yepez, e-print quant-ph/0210092.
[8] J. Yepez, preceding paper, Phys. Rev. A **74**, 042322 (2006).
[9] M. Pravia, E. Fortunato, Y. Weinstein, M. D. Price, G. Teklemariam, R. J. Nelson, Y. Sharf, S. Somaroo, C. H. Tseng, T. F. Havel, and D. G. Cory, Concepts Magn. Reson. **11**, 225–238 (1999).